Biosensors and Bioelectronics 24 (2009) 2352–2357

Contents lists available at ScienceDirect

Biosensors and Bioelectronics

journal homepage: www.elsevier.com/locate/bios

Bioelectrochemistry of hemoglobin immobilized on a sodium alginate-multiwall carbon nanotubes composite film

H.Y. Zhao[a], W. Zheng[a], Z.X. Meng[a], H.M. Zhou[a], X.X. Xu[a], Z. Li[a], Y.F. Zheng[a,b,*]

[a] Center for Biomedical Materials and Engineering, Harbin Engineering University, Harbin 150001, China
[b] Department of Advanced Materials and Nanotechnology, College of Engineering, Peking University, Beijing 100871, China

ARTICLE INFO

Article history:
Received 10 October 2008
Received in revised form 2 December 2008
Accepted 3 December 2008
Available online 9 December 2008

Keywords:
Sodium alginate-multiwall carbon nanotubes composite film
Hemoglobin
Direct electron transfer
Electrocatalysis
Biosensor

ABSTRACT

This study described the bioelectrochemistry of hemoglobin (Hb) at multiwall carbon nanotubes (MWCNTs) noncovalently functionalized with biopolymers of sodium alginate (SA). The characteristics of Hb/SA–MWCNTs composite film were studied by using FT-IR spectroscopy, UV–vis spectroscopy and electrochemical methods. Hb immobilized on SA–MWCNTs composite film retained its native secondary structure, achieved direct electron transfer with the apparent heterogeneous electron transfer rate constant (k_s) of $(9.54 \pm 0.883)\,s^{-1}$ and showed excellent bioelectrocatalytic activity to the reduction of hydrogen peroxide. The amperometric response of the biosensor varied linearly with the H_2O_2 concentration ranging from 40 to 200 μM, with a detection limit of 16.41×10^{-6} M (S/N = 3) and the good long-term stability. Finally, we applied this proposed method to investigate the concentration of hydrogen peroxide in real samples.

1. Introduction

The study of direct electron transfer of enzymes or proteins with electrodes can not only obtain valuable information about the mechanisms of electron transfer reactions in biological system, but also provide a platform for fabricating biosensors and biomedical devices without the addition of mediators or promoters (Reed and Hawkridge, 1987; Ye and Baldwin, 1988; Degani and Heller, 1989; Lotzbeyer et al., 1996; Rusling, 1998; Gorton et al., 1999; Sun et al., 2000; Fan et al., 2001; Lai and Bergel, 2002; Varma and Mitra, 2002; Liu et al., 2004a,b; Silva et al., 2005; Yu et al., 2005; Zheng and Zheng, 2007; Dodhia et al., 2008; ElKaoutit et al., 2008). So the direct electron transfer between redox proteins and the electrodes has aroused considerable interests in recent years. Hemoglobin is an iron-containing oxygen-transport metalloprotein in the mammals' red blood cells and has a molecular weight of 68 kDa (Matthew et al., 1979). The direct electron transfer between the Hb immobilized on the bare electrode or in the solution and the electrode is generally difficult due to the complex structure of its redox centers and the unfavorable orientations of Hb (Taniguchi et al., 1992). In order to overcome this problem, great efforts have been made to improve the direct electron transfer of protein by incorporating them into appropriate matrix such as ionic liquids (Yu et al., 2005), surfactant (Sun et al., 1999), biopolymers (Zheng et al., 2008a,b), hydrogels (Gregg and Heller, 1990), nanomaterials (Zheng and Zheng, 2007; Zheng et al., 2008c), etc., which have good biocompatibility for redox proteins immobilized on the electrode and can keep their bioactivities.

In recent years, nanomaterials have been investigated as substrates for immobilizing redox enzymes or proteins due to their superior structural stability and small sizes (Zhou et al., 2002; Li and Hu, 2003; Zheng et al., 2008c). Since their discovery in 1991, carbon nanotubes (CNT) have captured the imagination of scientists worldwide and been the focus of numerous investigations due to their unique structural and electronic properties. Despite of the extensive efforts made in the past, many potential applications of this exotic material still have not been realized in part because of the processing and manipulation difficulties. Therefore, much attempts have been made to circumvent such a problem mainly through covalent and noncovalent functionalization of the CNTs (O'Connell et al., 2001; Nguyen et al., 2002; Dyke and Tour, 2003; Stevens et al., 2003; Wang et al., 2003). However, the noncovalent approach is prone to be preferable compared with the covalent one because it preserves the unique structural and electronic properties of the CNTs.

Sodium alginate (SA) is a natural anionic polysaccharide and a linear binary copolymer consisting of linked 1,4-β-D-mannuronic

* Corresponding author at: Center for Biomedical Materials and Engineering, Harbin Engineering University, No.145, Na-Tong-Da Street, Nan-Gang District, Harbin 150001, China. Tel.: +86 451 82518644; fax: +86 451 82518644.
E-mail address: yfzheng@hrbeu.edu.cn (Y.F. Zheng).

0956-5663/$ – see front matter © 2008 Elsevier B.V. All rights reserved.
doi:10.1016/j.bios.2008.12.004

acid (M) and α-L-guluronic acid (G) residues (Holme et al., 2008). It has some unique properties such as non-toxicity, biocompatibility, biodegradability, chelating ability and hydrophilicity, and is an important biopolymer used to make microcapsules for drug delivery and immobilization of biocatalysts, wound dressing, tissue engineering (Choi et al., 1999; Orive et al., 2004; Prang et al., 2006). In this paper, we made use of the SA to noncovalent functionalize the MWCNTs by hydrophobic–hydrophobic interaction (Wang et al., 2002), and prepared SA–MWCNTs composite with excellent dispersion, finally actualized the direct electron transfer of the Hb co-assembled onto SA–MWCNTs composite film.

2. Experimental

2.1. Materials and apparatus

Multiwall carbon nanotubes (MWCNTs, diameter 10–30 nm, length 1–2 μm) were purchased from Shenzhen Nanotech Port Co., Ltd. (Shenzhen, China). Hemoglobin (Hb, from bovine blood, MW 66,000, lyophilized powder, the isoelectric point pI ~ 7.4 (Matthew et al., 1979) was purchased from Sigma and was used without additional purification. The hydrogen peroxide (30% (w/w)) and the SA were from Beijing Chemical Company (Beijing, China). The dilute solution of H_2O_2 was prepared daily. Aqueous solutions were prepared with doubly distilled water. Potassium dihydrogen orthophosphate (0.10 M) was used to prepare the supporting electrolyte and its pH value was adjusted to 7.0 using KOH. All other chemicals and solvents were at analytical grade and used without further purification.

FT-IR spectra were obtained on a PerkinElmer Spectrome 100 spectrometer (PerkinElmer Company, USA) at room temperature. UV–visible (UV–vis) absorption spectrum was carried out by using a 2550 spectrophotometer (Shimadzu, Japan).

Electrochemical measurements were carried out with a computer-controlled electrochemical analyzer (CHI 650C, CHI, Austin, TX) in a two-compartment and three-electrode cell containing 20 mL 0.10 M phosphate buffer (pH 7.0), which was used as the supporting electrolyte. The modified GC electrodes were used as working electrodes, a platinum spiral wire and a saturated calomel electrode (SCE) as auxiliary and reference electrode, respectively. For the experiments conducted under anaerobic condition, the electrolyte was bubbled with pure N_2 gas for more than 30 min and N_2 gas was kept flowing over the solution during the electrochemical measurements. All electrochemical measurements were performed at ambient temperature (18 ± 2 °C).

2.2. Preparation of the modified electrodes

The bare glassy carbon (GC, 3 mm-diameter) was first polished before use with emery paper (# 2000), 0.3 and 0.05 μm alumina slurry on a woollen cloth, and then cleaned under bath sonication for 10 min and finally thoroughly rinsed with distilled water.

The MWCNTs (2 mg) and SA (2 mg mL^{-1}) were mixed in aqueous solution and this mixture was sonicated for 0.5 h at room temperature to obtain a homogeneous and black dispersion containing 2.0 mg mL^{-1} MWCNTs. For the preparation of Hb/SA–MWCNTs/GC electrodes, a 4 μL of the dispersion was dip-coated onto the pretreated GC electrodes, followed by a period of standing in air until dry. Then the SA–MWCNTs/GC electrodes were immersed into 0.10 M phosphate buffer containing 20 mg mL^{-1} Hb for different times. The resulting electrodes (Hb/SA–MWCNTs/GC) were rinsed with distilled water prior to electrochemical measurements.

3. Results and discussion

3.1. Characterization of SA–MWCNTs and Hb/SA–MWCNTs composite film

It is known that MWCNTs is easily tend to aggregate in water (Fig. 1A) due to the van der Waals interaction between nanotubes (Zheng et al., 2006), indicating a poor solubility. However, compared with the pristine MWCNTs without any functionalization, the MWCNTs functionalized with SA can form homogeneous and black dispersion in aqueous solution, as shown in Fig. 1A. The homogeneous dispersion could be essentially stable for at least 2 weeks. As is known, the wrapping of CNTs by polymer with polar side-chains could lead to stable solutions of the corresponding polymer–CNTs complexes in water (Hirsch, 2002). Therefore, the MWCNTs bundles were also believed to be broken up by complex formation in the present study. Meanwhile, as one of the most ideal biocompatible materials, SA has good biocompatibility, which endows the MWCNTs noncovalently functionalized by SA with enhanced biocompatibility.

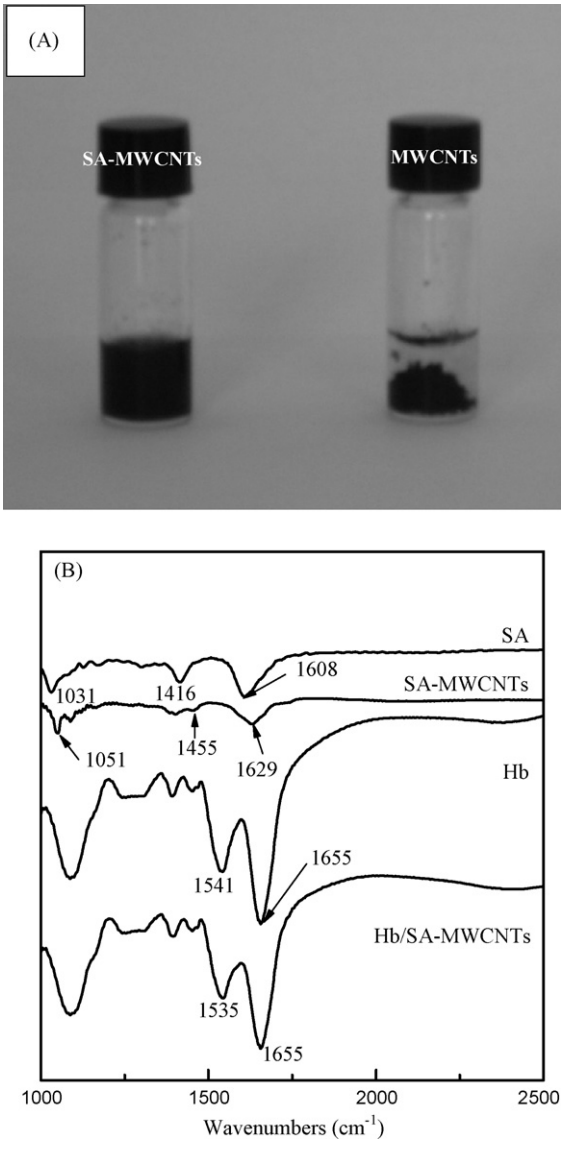

Fig. 1. (A) Photographs of 2 mg mL^{-1} SA–MWCNTs and MWCNTs dispersions and (B) FT-IR spectra of the SA, SA–MWCNTs, Hb and Hb/SA–MWCNTs samples.

Fig. 1B shows the FT-IR spectra of free SA and the SA–MWCNTs composite. The FT-IR spectra of the free SA exhibited its asymmetric stretching vibration of carboxylate O–C–O at 1608 cm^{-1}, the C–OH deformation vibration with contribution of O–C–O symmetric stretching vibration of carboxylate group at 1416 cm^{-1}, and the C–O stretching vibration of pyranose rings at 1031 cm^{-1}, respectively (Peniche et al., 1999; Leal et al., 2008). Moreover, these characteristic absorption bands of SA were observed in the spectrum of the SA–MWCNTs composite. On the other hand, the FT-IR spectrum of the SA was changed upon its adsorption onto the MWCNTs, which may be due to the strong interaction between SA and the MWCNTs.

The positions of the amide bands can provide information about secondary structure of polypeptide chain because their positions are more sensitive to protein peptide chain conformational change (Kauppinen et al., 1981). The amide I band (1700–1600 cm^{-1}) and the amide II band (1600–1500 cm^{-1}) are ascribed to the C–O stretching vibration of peptide linkages in the backbone of Hb and a combination of N–H bending and C–N stretching in Hb, respectively. We have employed FT-IR spectroscopy to investigate the structural variations of Hb immobilized into the SA–MWCNTs composite films, as shown in Fig. 1B. It can seen that the adsorption bands of amide I and amide II bands for native Hb were observed at 1655 and 1541 cm^{-1}, respectively. Similar characteristic peaks (1655 and 1535 cm^{-1}) were observed for the Hb immobilized on the Hb/SA–MWCNT composite film at this time. The similarity of the two spectra revealed that the Hb immobilized on the Hb/SA–MWCNT composite film almost retained its original structure. These results indicated that the SA–MWCNT composite film may provide a promising matrix for the enzyme immobilization and the biosensor fabrication.

Fig. 2 illustrates the UV–vis spectrum of the SA–MWCNTs, Hb and Hb/SA–MWCNTs films. The Soret absorption band of heme prosthetic group may provide the information on the tertiary structure of heme proteins, especially that of conformational change around the heme region (Theorell and Ehrenberg, 1951). As shown in Fig. 2A, the Soret band of the Hb entrapped in SA–MWCNT compound films was observed at 412 nm, shifting only 2 nm toward the red with the Soret band of 410 nm for native Hb film. Thus it can be concluded that the Hb entrapped in the SA–MWCNTs composite films could retain its native structure because the MWCNTs noncovalently functionalized with SA might have good biocompatibility. In addition, the absorbance at 412 nm was found to clearly increase with the increasing time of immersing the SA–MWCNTs composite films into Hb solution. Such phenomena could be reflective of the co-assembling process of Hb adsorbed into SA–MWCNTs compound films, forming biocompatible functional nanohybrids.

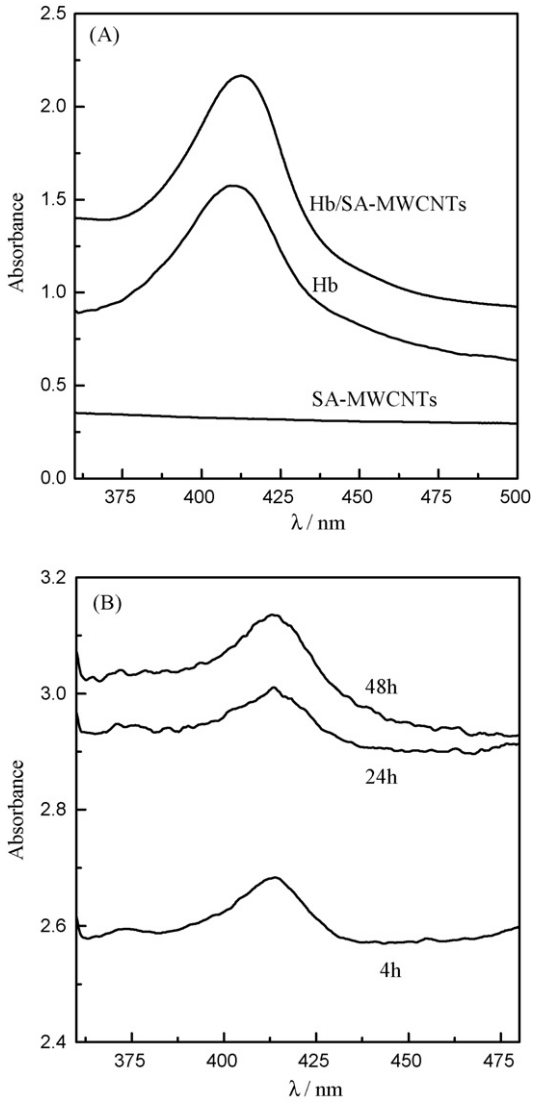

Fig. 2. UV–visible spectra of the SA–MWCNTs, Hb and Hb/SA–MWCNTs films on indium tin oxide sides (A) and SA–MWCNTs immersed in the Hb solution for different times (B).

3.2. Direct electrochemistry of Hb/SA–MWCNTs composite film

Fig. 3A shows the cyclic voltammograms (CVs) of the Hb immobilized into SA–MWCNTs composite film modified electrodes prepared by immersing the SA–MWCNTs/GC electrode in 0.10 M phosphate buffer containing 20 mg mL^{-1} Hb for different times. As can be seen from Fig. 3A, the CVs of Hb/SA–MWCNTs/GC electrodes in 0.10 M phosphate buffer solution of pH 7.0 at a scan rate of 100 mV s^{-1} gave a pair of well-defined redox peaks, the anodic peak potential (E_{pa}) and the cathodic peak potential (E_{pc}) were −0.32 and −0.39 V, respectively. The formal potential $E^{0'}$ (defined as the average of the anodic and cathodic peak potentials) was −0.36 V (vs. SCE) and the peak-to-peak separation (ΔE_p) was 70 mV at a scan rate of 100 mV s^{-1}, which was similar to that of Hb on other nanomaterials modified electrode previously reported (Yu et al., 2005; Shan et al., 2007; Zheng and Zheng, 2007; Zhu et al., 2007; Zheng et al., 2008c), indicating that direct electron transfer achieved between Hb and GC electrodes was realized in the microenvironment formed by SA–MWCNTs film. This may due to the three-dimensional architecture of the SA–MWCNTs composite film electrode. Moreover, the SA could let the Hb maintain its suitable conformation and activity, which made the direct electron transfer between the Hb and the electrode easy. Hence, it can be concluded that the SA was useful for solubilization, thereby avoided the aggregation of MWCNTs, and the SA–dispersed MWCNTs was useful for facilitating electron transfer of the proteins.

On the other hand, it can be easily found that the anodic and cathodic peak current obtained at the Hb/SA–MWCNTs/GC electrodes clearly increased with the increasing time of immersing the SA–MWCNTs/GC electrodes into Hb solution, suggesting that the amount of Hb increased gradually. This result was very consistent with that of UV–vis, which further indicated that the surface concentration of Hb increased with the increasing time during immersing the SA–MWCNTs composite films into Hb solution. Moreover, the peak current tended to be stable after 48 h immersing in the Hb solution because the Hb might reach saturation. Hence, an optimal immersion time of 48 h was selected for preparation in the following work.

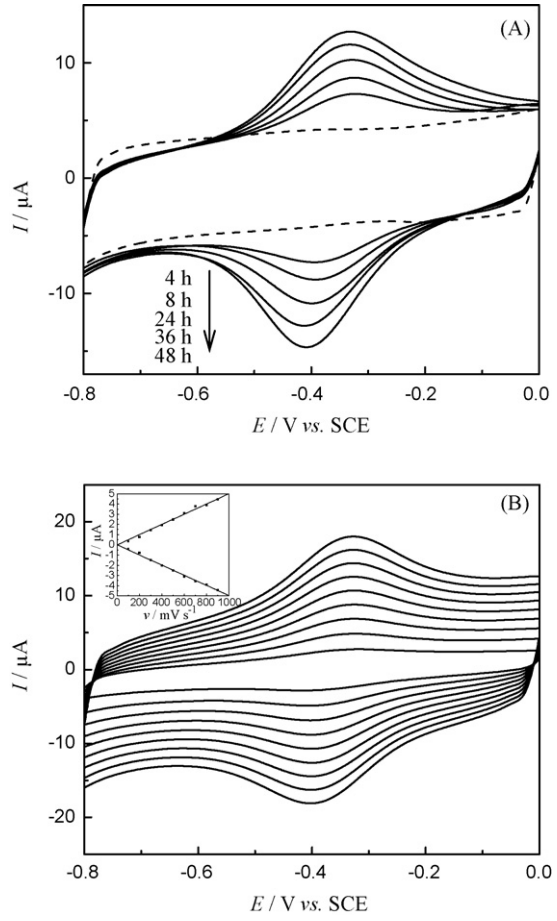

Fig. 3. (A) Cyclic voltammograms (CVs) obtained at SA–MWCNTs/GC (dashed line) and Hb/SA–MWCNTs/GC (solid line) electrodes in 0.10 M N_2-saturated phosphate buffer. The Hb/SA–MWCNTs/GC electrodes were prepared by immersing the SA–MWCNTs/GC electrode into 20 mg mL^{-1} Hb solution for different times of 4, 8, 24, 36, and 48 h (from inner to outer). (B) CVs obtained at Hb/SA–MWCNTs/GC electrode in 0.10 M N_2-saturated phosphate buffer at 100, 200, 300, 400, 500, 600, 700, 800 and 900 mV s^{-1} (from inner to outer). Inset showed a plot of cathodic and anodic peak currents against potential scan rate.

Fig. 3B shows the cyclic voltammograms for the redox of Hb entrapped in the SA–MWCNTs/GC modified electrodes at various scan rates in 0.10 M phosphate buffer (pH 7.0). It could be observed that the peak current increased along with the rising of scan rate from 100 to 900 mV s^{-1}, while the ΔE_p expanded slowly. Moreover, the cathodic and anodic peak currents increased linearly with the scan rate (not $v^{1/2}$), as shown in the inset of Fig. 3B.

The surface coverage (Γ) of Hb can be deduced according to the Faraday's law, $Q = nFA\Gamma$. Here F was Faraday's constant, Q could be obtained by integrating the cathodic peak of Hb, n and A stood for the number of electron transferred and the area of the electrode surface, respectively. The surface concentration of electroactive Hb at the Hb/SA–MWCNTs/GC electrodes was estimated to be $(3.98 \pm 0.249) \times 10^{-10}$ mol cm^{-2}.

In addition, when the scan rate exceeded 3 V s^{-1}, ΔE_p was more than 200 mV and the surface electrochemical reaction had become irreversible. In this case, the apparent heterogeneous electron transfer rate constant (k_s) could be calculated according to the equation derived Laviron for diffusionless CV as follows (Laviron, 1979):

$$E_{p,c} = E^{0'} + \frac{RT}{\alpha nF} \ln \frac{RTk_s}{\alpha nF} - \frac{RT}{\alpha nF} \ln v$$

$$E_{p,a} = E^{0'} - \frac{RT}{(1-\alpha)nF} \ln \frac{RTk_s}{(1-\alpha)nF} + \frac{RT}{(1-\alpha)nF} \ln v$$

$$\Delta E_p = \frac{RT}{\alpha(1-\alpha)nF} \ln v + \frac{RT}{\alpha(1-\alpha)nF} \times \left\{ \alpha \ln(1-\alpha) + (1-\alpha) \ln \alpha - \ln \frac{RT}{nF} - \ln k_s \right\}$$

where α was the electron transfer coefficient, k_s was the apparent heterogeneous electron transfer rate constants, and v was the scan rate. The value of k_s was calculated to be (9.54 ± 0.883) s^{-1}, which was higher than that of Hb immobilized on a nano-CdS/Nafion composite film (0.291 s^{-1}) (Sun et al., 2008) and on a CHT/nano-$CaCO_3$ composite film (1.8 s^{-1}) (Shan et al., 2007), indicating that the Hb immobilized into SA–MWCNTs composite film achieved a fast electron transfer process. This may because that the SA–MWCNTs may act as electron bridges or connectors between those neighboring Hb molecules with a relatively large distance, making the electron hopping between these Hb molecules become possible and more Hb molecules become electroactive (Zhang and Hu, 2007).

The dependence of the electrochemical behavior of Hb/SA–MWCNTs/GC modified electrodes on the pH of the electrolyte solution was further investigated. The result showed that an increase in pH from 5 to 9 in phosphate buffers led to a negative shift of the anodic and cathodic peak potentials for the Hb/SA–MWCNTs/GC modified electrodes. Moreover, E_{pa}, E_{pc} and $E^{0'}$ exhibited linear relationship with the pH value in the range of pH 5.0–9.0, the slopes of −43.83 mV pH^{-1}, −44.80 mV pH^{-1} and −45.77 mV pH^{-1}, respectively. These values was similar to those measured at Hb/PAM-chitosan electrode (Zeng et al., 2007), Chi/{UND/Hb}$_3$ electrode (Zhu et al., 2007) and Hb/meso-Al_2O_3 modified electrode (Yu et al., 2007), which were smaller than the theoretical value of −57.6 mV pH^{-1} at 18 °C for the reaction of one electron coupled one proton. It is suggested that the groups near the heme iron made an impact on redox potential. Thus, the protonation of distal or proximal histidines, or the protonation of the water molecule coordinated to the central iron might be responsible for the pH dependence of $E^{0'}$ (Yamazaki et al., 1978; Liu et al., 2004a,b).

3.3. H_2O_2 biosensor based on Hb/SA–MWCNTs composite film

The detection of hydrogen peroxide (H_2O_2) in environmental, industrial, chemical, food, and pharmaceutical fields is of great importance. Compared with other methods, such as titrimetry, spectrometry and chemiluminescence methods, the electrochemical technique for the determination of H_2O_2 coupled with the intrinsic selectivity and sensitivity of enzymatic reactions is promising for the fabrication of simple and low-cost enzyme sensors (Razola et al., 2002). Fig. 4A shows the cyclic voltammograms of the Hb/SA–MWCNTs/GC electrode by adding hydrogen peroxide. As can be seen from Fig. 4A, when the H_2O_2 was added into phosphate buffer, the cathodic peak currents for the Hb-immobilized SA–MWCNTs/GC electrodes at about −0.40 V increased dramatically with the decrease of the anodic peak because Hb–Fe^{II} can be oxidized by H_2O_2 and transferred to Hb–Fe^{III} quickly when Hb–Fe^{III} is directly electrochemical reduced to Hb–Fe^{II} (Liu and Hu, 2005; Zhang et al., 2007). Moreover, when the concentration of H_2O_2 increased gradually in the phosphate buffer, the cathodic peak currents was further increased, indicating that the immobilized Hb exhibited excellent electrocatalytic activity toward the reduction of H_2O_2.

Fig. 4B shows an example of the chronoamperometric response of the Hb/SA–MWCNTs/GC electrodes to different concentrations of H_2O_2 at an applied potential of −0.40 V. Obviously, the electrocat-

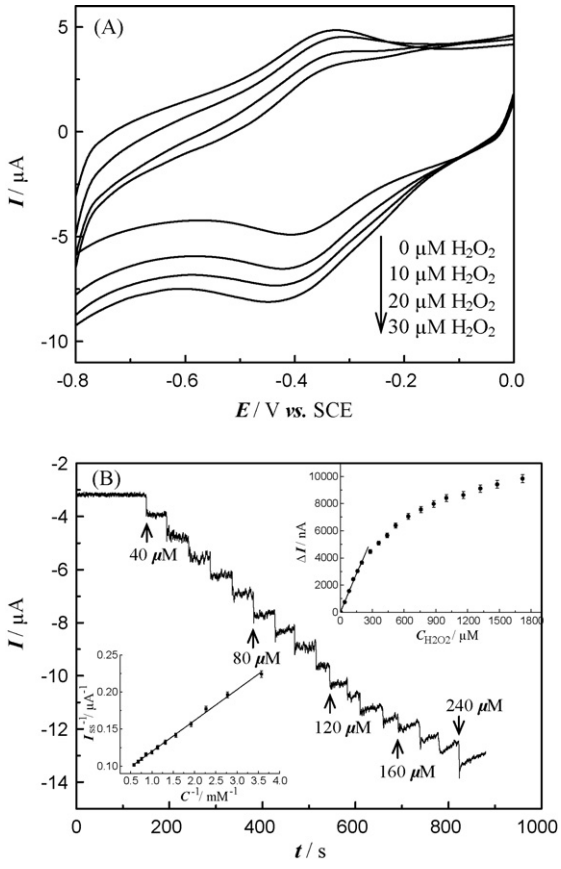

Fig. 4. (A) CVs of Hb/SA–MWCNTs/GC electrode in 0.10 M pH 7.0 phosphate buffer containing different contents of H_2O_2. (B) Amperometric responses of Hb/SA–MWCNTs/GC electrode in stirred solutions to the successive additions of H_2O_2. Insets are the calibration curve (top right) and corresponding Lineweaver–Burk plot (left side).

alytic current of the biosensor increased with each addition of H_2O_2 to the solution. Moreover, the current reached its maximum value within 10 s after each addition of H_2O_2, which suggested that the biosensor can respond rapidly to the change of the concentration of H_2O_2. As can be seen from the top right of Fig. 4B, the linear range of this biosensor to H_2O_2 concentration was between 40 and 200 μM which can be described by a linear regression equation of ΔI (nA) = 42.86 + 15.87C (μM), (R = 0.995). From the slope of the regression equation, the detection limit of the biosensor was 16.41 μM based on noise ratio of 3. When the concentration of H_2O_2 was higher than 200 μM, a response plateau was observed, representing the feature of the Michaelis–Menten kinetic mechanism. According to the Lineweaver–Burk form of the Michaelis–Menten equation (Kamin and Wilson, 1980): $1/I_{ss} = (1/I_{max}) + (K_m^{app}/I_{max}C)$. Here I_{ss} was the steady-state current after the addition of a substrate and obtained from amperometric experiments, I_{max} was the maximum current under saturated substrate conditions, C was the concentration of the substrate, and K_m^{app} was the apparent Michaelis–Menten constant and was independent of the enzyme concentration. A value of 0.533 mM for K_m^{app} was obtained by the analysis of slope and intercept of the reciprocals of the steady-state current versus H_2O_2 concentration. Compared to the literature report of H_2O_2 biosensors based on carbon nanotubes (Chen et al., 2007; Guo et al., 2008), the detection limit and K_m^{app} of the present biosensor was relatively higher, but these values were markedly smaller than that of biosensors based on other nanomaterials (Wang et al., 2004; Feng et al., 2006; Shan et al., 2007).

To further assess the possible application of our proposed biosensors for real analytical usefulness, we measured the concentration of H_2O_2 in different disinfectant samples. The disinfectant samples were firstly diluted with phosphate buffer (pH 7.0) before the detection, in order to make the concentration of H_2O_2 locating in the detection limit range. And then, they were measured using the above method and classical permanganate titration method, respectively. The results were shown in Table 1, from which it can be seen that the value obtained by the proposed method was consistent with that obtained by the classical permanganate titration method. The relative standard deviations between two methods were in the range of −2.20 to 2.34%. Therefore, it can be concluded that the present biosensor is reliable and effective for future applications, at least for the detection of the concentration of H_2O_2 in disinfectant sample.

Table 1
Measurement of H_2O_2 (mol L^{-1}) in disinfectant samples (n = 5).

Groups	H_2O_2 biosensor	$KMnO_4$ titration
1	0.65 ± 0.099	0.635
2	0.92 ± 0.054	0.925
3	0.71 ± 0.073	0.726

For the biosensor application of Hb/SA–MWCNTs, the stability of biosensor is also very critical. When the H_2O_2 biosensor had been stored in a 0.10 M phosphate buffer for 3 weeks at 4 °C, the biosensor retained over 90% response of its initial sensitivity to the reduction of H_2O_2, demonstrating its good long-term stability. The reproducibility of the biosensor was examined in 50 μM H_2O_2, and the relative standard deviation was approximately 2.48% for five successive assays.

4. Conclusions

The present paper demonstrated that the MWCNTs noncovalently functionalized by the biopolymer of SA essentially increased the solubility of MWCNTs in water and improved its biocompatibility, which substantially facilitated the bioelectrochemical applications of the MWCNTs. The direct electron transfer of Hb immobilized SA–MWCNTs composite film was largely facilitated and showed the excellent bioelectrocatalytic activities toward the reduction of hydrogen peroxide. Such kind of SA–MWCNTs composite film could find a potential application in the biosensing field.

Acknowledgement

This work was supported by the National Natural Science Foundation of China (No. 20805010).

References

Chen, S., Yuan, R., Chai, Y., Zhang, L., Wang, N., Li, X., 2007. Biosens. Bioelectron. 22, 1268–1274.
Choi, Y.S., Hong, S.R., Lee, Y.M., Song, K.W., Park, M.H., Nam, Y.S., 1999. Biomaterials 20, 409–417.
Degani, Y., Heller, A., 1989. J. Am. Chem. Soc. 111, 2357–2358.
Dodhia, V.R., Sassone, C., Fantuzzi, A., Nardo, G.D., Sadeghi, S.J., Gilardi, G., 2008. Electrochem. Commun. 10, 1744–1747.
Dyke, C.A., Tour, J.M., 2003. J. Am. Chem. Soc. 125, 1156–1157.
ElKaoutit, M., Naranjo-Rodriguez, I., Dominguez, M., Hernandez-Artiga, M.P., Bellido-Milla, D., Hidalgo-Hidalgo de Cisneros, J.L., 2008. Electrochim. Acta 53, 7131–7137.
Fan, C., Wang, H., Sun, J., Wagner, G., Li, G., 2001. Anal. Chem. 73, 2850–2854.
Feng, J.J., Xu, J.J., Chen, H.Y., 2006. Electrochem. Commun. 8, 77–82.
Gorton, L., Lindgren, A., Larsson, T., Munteanu, F.D., Ruzgas, T., Gazaryan, I., 1999. Anal. Chim. Acta 400, 91–108.
Gregg, B.A., Heller, A., 1990. Anal. Chem. 62, 258–263.
Guo, C., Hu, F., Li, C., Shen, P.K., 2008. Biosens. Bioelectron. 24, 819–824.
Hirsch, A., 2002. Angew. Chem. Int. Ed. 41, 1853–1859.
Holme, H.K., Davidsen, L., Kristiansen, A., Smidsr, O., 2008. Carbohyd. Polym. 73, 656–664.
Kamin, R.A., Wilson, G.S., 1980. Anal. Chem. 52, 1198–1205.

Kauppinen, J.K., Moffate, D.J., Mantsch, H.H., Lameron, D.G., 1981. Appl. Spectrosc. 35, 271–276.
Lai, M.E., Bergel, A., 2002. Bioelectrochemistry 55, 157–160.
Laviron, E., 1979. J Electroanal. Chem. 61, 19–28.
Leal, D., Matsuhiro, B., Rossi, M., Caruso, F., 2008. Carbohyd. Res. 343, 308–316.
Li, Z., Hu, N.F., 2003. J. Electroanal. Chem. 558, 155–165.
Liu, H., Hu, N., 2005. J. Phys. Chem. B 109, 10464–10473.
Liu, H., Tian, Z., Lu, Z., Zhang, Z., Zhang, M., Pang, D., 2004a. Biosens. Bioelectron. 20, 294–304.
Liu, S.Q., Dai, Z.H., Chen, H.Y., Ju, H.X., 2004b. Biosens. Bioelectron. 19, 963–969.
Lotzbeyer, T., Schuhmann, W., Schmidt, H., 1996. Sens. Actuators B: Chem. 33, 50–54.
Matthew, J.B., Hanania, G.I.H., Gurd, F.R.N., 1979. Biochemistry 18, 1919–1928.
Nguyen, C.V., Delzeit, L., Cassell, A.M., Li, J., Han, J., Meyyappan, M., 2002. Nano Lett. 2, 1079–1081.
O'Connell, M.J., Boul, P., Ericson, L.M., Huffinan, C., Wang, Y., Haroz, E., Kuper, C., Tour, J., Ausman, K.D., Smalley, R.E., 2001. Chem. Phys. Lett. 342, 265–271.
Orive, G., Ponce, S., Hernandez, R.M., 2004. Biomaterials 23, 3825–3831.
Peniche, C., Arguelles-Monal, W., Davidenko, N., Sastre, R., Gallardo, A., Roman, J.S., 1999. Biomaterials 20, 1869–1878.
Prang, P., Muller, R., Eljaouhari, A., Heckmann, K., Kunz, W., Webber, T., Faber, C., Vroemen, M., Bogdahn, U., Weidner, N., 2006. Biomaterials 27, 3560–3569.
Razola, S.S., Ruiz, B.L., Diez, N.M., Mark, H.B., Kauffmann, J.-M., 2002. Biosens. Bioelectron. 17, 921–928.
Reed, D.E., Hawkridge, F.M., 1987. Anal. Chem. 59, 2334–2339.
Rusling, J.F., 1998. Acc. Chem. Res. 31, 363–369.
Shan, D., Wang, S.X., Xue, H.G., Cosnier, S., 2007. Electrochem. Commun. 9, 529–534.
Silva, C.C., Rocha, H.H.B., Freire, F.N.A., Santos, M.R.P., Saboia, K.D.A., Goes, J.C., Sombra, A.S.B., 2005. Mater. Chem. Phys. 92, 260–268.
Stevens, J.L., Huang, A.Y., Peng, H., Chian, I.W., Khabashesku, V.N., Margrave, J.L., 2003. Nano Lett. 3, 331–336.
Sun, H., Ma, H., Hu, N., 1999. Bioelectrochem. Bioenerg. 49, 1–10.
Sun, H., Hu, N., Ma, H., 2000. Electroanalysis 12, 1064–1070.
Sun, W., Wang, D., Li, G., Zhai, Z., Zhao, R., Jiao, K., 2008. Electrochim. Acta 53, 8217–8221.
Taniguchi, I., Watanabe, K., Tominaga, M., Hawkridge, F.M., 1992. J. Electroanal. Chem. 333, 331–338.
Theorell, H., Ehrenberg, A., 1951. Acta Chem. Scand. 5, 823–848.
Varma, S., Mitra, C.K., 2002. Electrochem. Commun. 4, 151–157.
Wang, J., Musameh, M., Lin, Y., 2003. J. Am. Chem. Soc. 125, 2408–2409.
Wang, Q.L., Lu, G.X., Yang, B.J., 2004. Biosens. Bioelectron. 19, 1269–1275.
Wang, X., Liu, Y., Qiu, W., Zhu, D., 2002. J. Mater. Chem. 12, 1636–1639.
Yamazaki, I., Araiso, T., Hayashi, Y., Yamada, H., Makino, R., 1978. Adv. Biophys. 11, 249–281.
Ye, J., Baldwin, R.P., 1988. Anal. Chem. 60, 2263–2268.
Yu, P., Lin, Y., Xiang, L., Su, L., Zhang, J., Mao, L., 2005. Langmuir 21, 9000–9006.
Yu, J., Ma, J., Zhao, F., Zeng, B., 2007. Electrochim. Acta 53, 1995–2001.
Zhang, H., Hu, N., 2007. J. Phys. Chem. B 111, 10583–10590.
Zhang, L., Zhang, Q., Li, J., 2007. Electrochem. Commun. 9, 1530–1535.
Zeng, X., Wei, W., Li, X., Zeng, J., Wu, L., 2007. Bioelectrochemistry 71, 135–141.
Zheng, W., Li, Q., Su, L., Yan, Y., Zhang, J., Mao, L., 2006. Electroanalysis 18, 587–594.
Zheng, W., Zheng, Y.F., 2007. Electrochem. Commun. 9, 1619–1623.
Zheng, W., Li, J., Zheng, Y.F., 2008a. Biosens. Bioelectron. 23, 1562–1566.
Zheng, W., Li, J., Zheng, Y.F., 2008b. J. Electroanal. Chem. 621, 69–74.
Zheng, W., Zheng, Y.F., Jin, K.W., Wang, N., 2008c. Talanta 74, 1414–1419.
Zhou, Y.L., Li, Z., Hu, N.F., Zeng, Y.H., Rusling, J.F., 2002. Langmuir 18, 8573–8579.
Zhu, J., Shi, C., Xu, J., Chen, H., 2007. Bioelectrochemistry 71, 243–248.